Letter

Non-Hermitian boundary spectral winding

Zuxuan Ou,[1] Yucheng Wang,[2,3,4] and Linhu Li[1,*]

[1]*Guangdong Provincial Key Laboratory of Quantum Metrology and Sensing, and School of Physics and Astronomy, Sun Yat-Sen University (Zhuhai Campus), Zhuhai 519082, China*

[2]*Shenzhen Institute for Quantum Science and Engineering, Southern University of Science and Technology, Shenzhen 518055, China*

[3]*International Quantum Academy, Shenzhen 518048, China*

[4]*Guangdong Provincial Key Laboratory of Quantum Science and Engineering, Southern University of Science and Technology, Shenzhen 518055, China*

(Received 31 October 2022; revised 24 March 2023; accepted 27 March 2023; published 7 April 2023)

Spectral winding of complex eigenenergies represents a topological aspect unique in non-Hermitian systems, which vanishes in one-dimensional (1D) systems under the open boundary conditions (OBC). In this Letter, we discover a boundary spectral winding in two-dimensional non-Hermitian systems under the OBC, originating from the interplay between Hermitian boundary localization and non-Hermitian nonreciprocal pumping. Such a nontrivial boundary topology is demonstrated in a non-Hermitian breathing Kagome model with a triangle geometry, whose 1D boundary mimics a 1D non-Hermitian system under the periodic boundary conditions with nontrivial spectral winding. In a trapezoidal geometry, this boundary spectral winding can even coexist with corner accumulation of edge states, instead of extended ones along the 1D boundary of a triangle geometry. An OBC type of hybrid skin-topological effect may also emerge in a trapezoidal geometry, provided the boundary spectral winding completely vanishes. By studying the Green's function, we unveil that the boundary spectral winding can be detected from a topological response of the system to a local driving field, offering a realistic method to extract the nontrivial boundary topology for experimental studies.

DOI: 10.1103/PhysRevB.107.L161404

I. INTRODUCTION

Non-Hermitian systems can support not only topological phases with boundary states protected by conventional band topology [1,2], but also spectral winding topology of complex eigenenergies which has no Hermitian analog. Nontrivial spectral winding generally emerges in many non-Hermitian lattices under the periodic boundary conditions (PBC), and vanishes when the boundary is opened, i.e., the open boundary conditions (OBC), resulting in the non-Hermitian skin effect (NHSE) where bulk states become skin localized at the system's boundary [3–7]. One of the most noteworthy consequences of the interplay between conventional and spectral winding topology is the breakdown of conventional topological bulk-boundary correspondence [8,9], which has led to recent extensive investigations of its recovery through several different methods [3,10–14] and many other exciting phenomena induced by NHSE and spectral winding topology [15–37].

In contemporary literature, spectral winding topology is most clearly studied in one-dimensional (1D) systems, as by definition it corresponds to 1D trajectories in the two-dimensional (2D) complex-energy plane, which cannot be straightforwardly generalized into higher spatial dimensions. On the other hand, being a boundary phenomenon, NHSE in two or higher dimensions is also far more sophisticated than in one dimension, possessing many variations associated with different boundaries and defects due to their richer geometric structures [38–43]. In this Letter, we unveil an exotic aspect of spectral winding in higher dimensions, namely, nontrivial spectral winding for 1D boundary states of 2D lattices under the OBC, in sharp contrast to our knowledge of vanishing spectral winding topology of OBC systems. This enigmatic phenomenon has been noticed in recent literature [44,45], yet the mechanism behind it remains ambiguous. Here we find that its emergence originates from the interplay between Hermitian boundary localization and a non-Hermitian chiral pumping along the boundary, i.e., asymmetric hoppings with stronger amplitudes toward a chiral direction [see Fig. 1(a) for an illustration]. A similar mechanism is known to be responsible for the hybrid skin-topological effect (HSTE) [46–49], a type of higher-order NHSE with topological protection [44,50,51], which induces corner skin-topological localization in 2D lattices. Interestingly, our example model of a non-Hermitian breathing Kagome lattice can support both nontrivial boundary spectral winding and an OBC type of HSTE under the same parameters, but with different triangle and trapezoidal geometries, where the chiral pumping is forbidden by boundary geometry of the latter case. These two phenomena represent different types of nontrivial higher-order non-Hermitian topological properties and require rather different geometric properties for 1D boundaries, unlike the bulk-geometry-dependent NHSE in two or higher dimensions [42]. In the intermedia regime between these two scenarios, nontrivial boundary spectral winding may even coincide with a weak corner localization, indicating a coexistence of the seemingly contradictory boundary spectral winding and HSTE. Moreover, we discover that this boundary spectral

*lilh56@mail.sysu.edu.cn

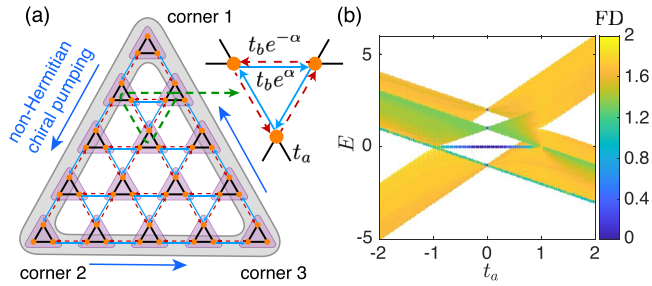

FIG. 1. (a) A sketch of the non-Hermitian breathing Kagome lattice with $L = 5$ rows of unit cells. The gray area represents the first-order boundary of the system, which gives the effective boundary Hamiltonian discussed latter. Blue arrows indicate the direction of non-Hermitian chiral pumping along the boundary. (b) Energy spectrum vs t_a, for the system with a triangle geometry in the Hermitian limit of $\alpha = 0$. Eigenenergies are marked by different colors according to their corresponding FD. Other parameters are $t_b = 1$ and $L = 30$.

winding can be detected from a topological response to a driving field when locally perturbing the 2D system, providing a feasible method to extract the nontrivial boundary topology from realistic non-Hermitian systems.

II. NON-HERMITIAN BREATHING KAGOME MODEL

We consider a non-Hermitian breathing Kagome model with asymmetric intracell hoppings [52] as shown in Fig. 1(a), with its bulk Hamiltonian given by

$$H(\mathbf{k}) = \begin{pmatrix} 0 & t_a + t_b^+ e^{-ik_1} & t_a + t_b^- e^{ik_3} \\ t_a + t_b^- e^{ik_1} & 0 & t_a + t_b^+ e^{-ik_2} \\ t_a + t_b^+ e^{-ik_3} & t_a + t_b^- e^{ik_2} & 0 \end{pmatrix}, \quad (1)$$

where $k_1 = -k_x/2 - \sqrt{3}k_y/2, k_2 = k_x, k_3 = -k_x/2 + \sqrt{3}k_y/2$, and $t_b^{\pm} = t_b e^{\pm\alpha}$ represent asymmetric intercell (downward triangle) hopping parameters, and t_a is the amplitude of intracell (upward triangle) Hermitian hopping. Here we set $t_b = 1$ as the unit energy. In the Hermitian scenario with $\alpha = 0$, the Kagome lattice model supports both first-order edge states and second-order corner states in certain parameter regimes, as shown in Fig. 1(b) where different bulk and boundary states are characterized by different values of their fractal dimension (FD), defined as

$$D_{\text{frac}} = -\ln\left[\sum_{\mathbf{r}} |\psi_{n,\mathbf{r}}|^4\right] \Big/ \ln\sqrt{3N}, \quad (2)$$

with $\psi_{n,\mathbf{r}}$ the wave amplitude at position $\mathbf{r}$ of the nth eigenstate, and N the total number of unit cells. In a triangle geometry, $N = (1 + L)L/2$ with L the number of rows of unit cells in the lattice. A 2D bulk state and a 1D edge state in our system shall have their FD close to 2 and 1, respectively. As seen in Fig. 1(b), the breathing Kagome lattice supports 1D edge states (represented by green color for $D_{\text{frac}} \simeq 1.2$) in a large parameter regime.

III. DESTRUCTIVE INTERFERENCE OF NONRECIPROCITY AND BOUNDARY SPECTRAL WINDING

By construction, the model can be viewed as a combination of three sets of non-Hermitian Su-Schrieffer-Heeger (SSH) chains [3,53–55] along different directions. Specifically, the three non-Hermitian SSH chains are chosen to be identical, resulting in a C_3 rotation symmetry of the system, as shown in Fig. 1(a). In this way, the asymmetric hoppings along the three directions form a closed loop and balance out in each unit cell, leading to a destructive interference of nonreciprocity in the bulk. The system is thus net reciprocal even in the presence of asymmetric hoppings. As seen in Fig. 2(a), FD is close to 2 for eigenstates in three bulk bands (yellow color) for the system with a triangle geometry, indicating the absence of NHSE for bulk states. Consistently, the summed bulk distribution, defined as

$$\rho_{\text{bulk}}(\mathbf{r}) = \sum_{n\in\text{bulk}} |\psi_{n,\mathbf{r}}|^2$$

with summation running over all eigenstates in the bulk bands, also distributes uniformly in the 2D bulk [Fig. 2(b)]. On the other hand, first-order edge states distribute mostly along 1D edges, and are subjected to a net non-Hermitian nonreciprocal pumping. The same mechanism is known to induce the HSTE in different square and honeycomb lattices. However, in our model with a triangle geometry, the destructive interference of nonreciprocity limits the choices of the nonreciprocal directions and forbids the HSTE. Namely, in the presence of destructive interference of nonreciprocity along three directions, a triangle lattice must have chiral nonreciprocal pumping along its 1D boundary, hence it is impossible to have two edges with nonreciprocity toward their shared corner. Consequently, we anticipate no hybrid skin-topological corner mode to appear in our system.

As verified in our numerical calculations, first-order edge states are indeed extended along 1D edges, as shown in Fig. 2(c) by the summed edge distribution

$$\rho_{\text{edge}}(\mathbf{r}) = \sum_{n\in\text{edge}} |\psi_{n,\mathbf{r}}|^2$$

with summation running over all edge states. Interestingly, a nontrivial spectral winding is seen to emerge for edge states, even when the system is under OBC [Fig. 2(a)]. To understand its emergence, we note that these edge states inhabit within the edges of a 2D lattice, which form an effective 1D boundary system without an open boundary, analogous to a 1D nonreciprocal system under PBC. By taking the edges of the 2D lattice as a 1D system decoupled from the 2D bulk, we find that its spectrum is almost identical to that of the first-order edge states of the original 2D system, as shown in Fig. 2(d). As seen in Fig. 2(e), their eigenstates display a slightly different but still extended distribution, as shown by $\rho_{\text{eff}} = \sum_n |\psi_{n,x}^{\text{1D}}|^2$ with $\psi_{n,x}^{\text{1D}}$ the wave amplitude at position x of the nth eigenstate of the 1D boundary system. Thus, the origin of nontrivial boundary spectral winding in our model can be qualitatively understood from this 1D boundary system. Note that, in contrast to an actual 1D PBC system, 1D edges of our 2D model possess an extra lattice site in each corner,

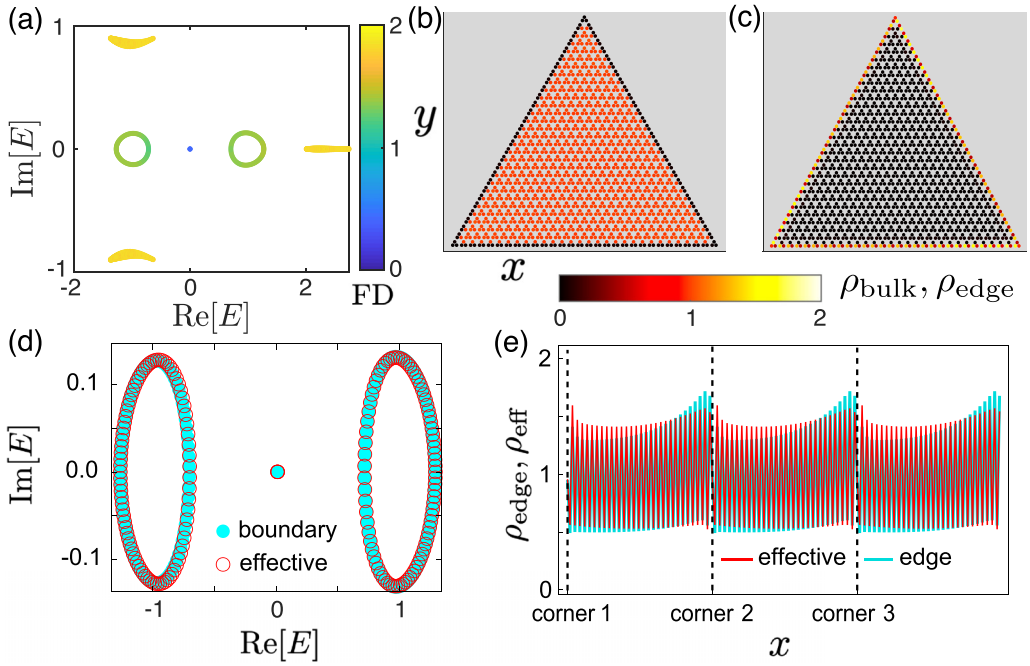

FIG. 2. (a) Energy spectrum under the OBC, where colors indicate the FD of each eigenstate. (b), (c) Summed distribution of bulk states and edge states, respectively. (d) Spectra of edge states for the 2D lattice (cyan dots) as in (a), and 1D effective boundary system corresponding to the gray area in Fig. 1(a) (red circles). (e) Summed distribution of edge states for the 2D lattice (cyan), and of all eigenstates for the 1D boundary system (red). Parameters are $t_a = 0.25, t_b = 1, \alpha = 0.5,$ and $L = 30$.

acting as impurities to the 1D effective model. As a result, we observe weak eigenstate accumulations toward these corners both for the edge states of the 2D model and for the effective 1D boundary system [Fig. 2(e)].

IV. TRAPEZOIDAL LATTICES AND AN OBC TYPE OF HYBRID SKIN-TOPOLOGICAL LOCALIZATION

In the triangle lattice, the emergence of nontrivial boundary spectral winding relies on the chiral nonreciprocal pumping along the 1D boundary. To further confirm this mechanism, here we break the chiral pumping channel by removing the top few rows of lattice sites from the triangle lattice. Specifically, we start from a triangle lattice with L unit cells along its bottom row, then remove the top M rows of unit cells and the top lattice sites of unit cells in the $M + 1$ row. A sketch of $L = 5$ and $M = 2$ is shown in Fig. 3(a). In the resultant trapezoidal lattices, the top row of lattice sites does not form complete upward unit cells, and asymmetric hoppings between these sites have stronger amplitudes toward the opposite chiral direction of the rest three edges, blocking the chiral pumping channel circulating the 2D lattice.

Intuitively, two domain walls are formed between top and remaining edges at corners 1 and 4, which shall lead to the emergence of HSTE in the trapezoidal geometry of our model. Yet its behaviors cannot be simply understood from this domain-wall picture. To see this, we may redefine a unit cell as a downward triangle, i.e., the green dashed line in Fig. 1(a) (see Supplemental Material [56] for further discussion of different definitions of unit cells). Then, when excluding the boundary lattice sites of left, right, and bottom edges, the remaining part of a trapezoidal lattice is formed only by intact unit cells. Therefore the top geometric edge of a trapezoidal lattice is more closely related to the physical bulk, and shall be considered as a part of it. In return, the effective 1D boundary no longer forms a closed loop. Indeed, as observed in Fig. 3(b) with $L = 30$ and $M = 20$, bulk states of the system show vanishing distribution only along the left, right, and bottom edges. On the other hand, edge states in this system exhibit a clear accumulation at the top-right corner (corner 4) for the chosen parameters, analogous to the behavior of a 1D non-Hermitian OBC system with the NHSE.

To further understand the boundary behaviors, we demonstrate the energy spectra for lattices with different sizes in Figs. 3(d)–3(f), with insets illustrating the distributions of their edge states and of a 1D boundary system under the OBC [i.e., the gray area in Fig. 3(a)]. In Fig. 3(d), the top $M = 5$ rows of unit cells are removed from a triangle lattice with $L = 30$. The resultant system shows a nontrivial boundary spectral winding in its complex spectrum, yet its edge states already become corner localized (with FD close to zero) and accumulate at corner 4. However, their accumulating strength is considerably weaker than that of skin states of the effective 1D OBC system. Such observations are analogous to the scale-free localization induced by impurities in a 1D non-Hermitian chain, where a boundary impurity connects the 1D chain head to the tail, resulting in an impurity boundary condition (IBC) between the OBC and PBC [31]. In our trapezoidal lattice, the top row of lattice sites can be viewed as impurities connecting the two ends (i.e., corners 1 and 4) of the 1D edges, mimicking the IBC that gives rise to the scale-free localization.

In Fig. 3(e), we demonstrate results with the same number of unit cells in the bottom row ($L = 30$), but removing the top $M = 10$ rows from a triangle lattice. Its edge states still

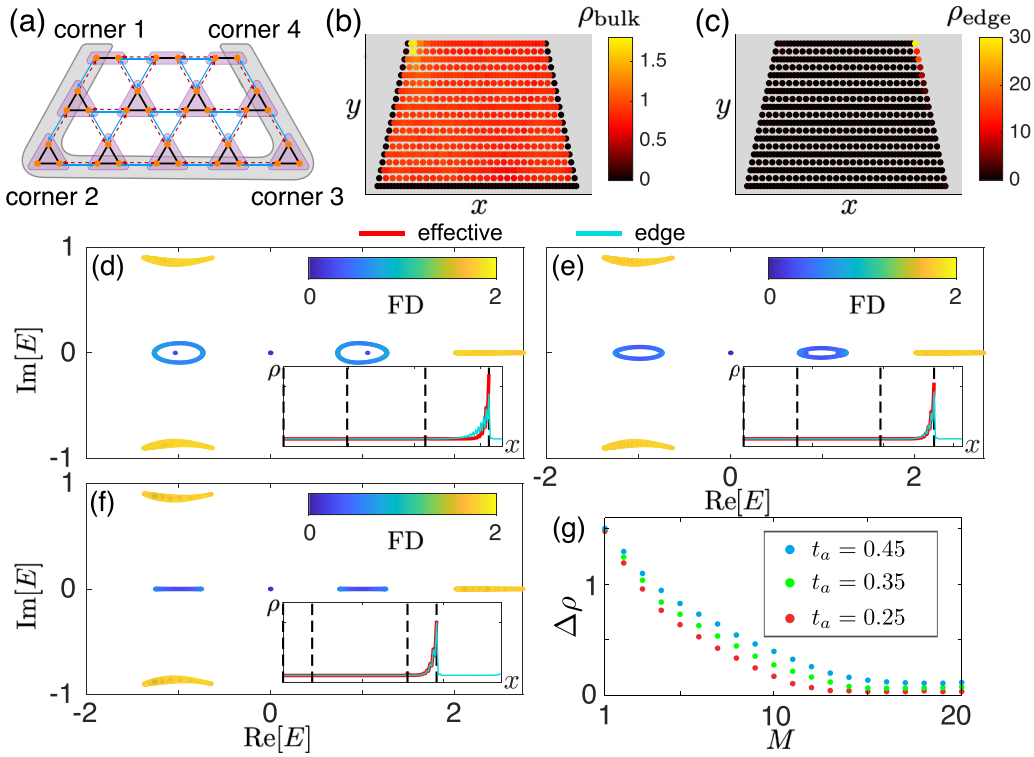

FIG. 3. (a) A sketch of a trapezoidal lattice of the non-Hermitian breathing Kagome model. (b), (c) Summed distribution of bulk states and edge states, respectively, with $L = 30$ and $M = 20$. (d)–(f) Energy spectra under OBC with $L = 30$ and $M = 5$, 10, and 20, respectively, where colors indicate the FD of each eigenstate. Summed distributions of edge states for the 2D trapezoidal lattice in (d) and (e) are illustrated in their insets (cyan), together with those of all eigenstates for the 1D boundary system (red). Dashed lines correspond to corners 1 to 4 from left to right, respectively. (g) $\Delta\rho = \sum_x |\rho_{\text{eff}} - \rho_{\text{edge}}|/L_{\text{eff}}$ as a function of M, for several different values of t_a. $t_a = 0.25$ is chosen in (b)–(f). Other parameters are $t_b = 1$ and $\alpha = 0.5$.

form a loop spectrum in the complex plane, yet their distribution becomes closer to the skin states of the corresponding 1D boundary system under the OBC. Finally, when further removing more rows from the triangle lattice [$M = 20$ in Fig. 3(f)], the boundary spectral winding eventually vanishes, and the distribution of edge states becomes almost identical to the skin states. It indicates that the boundary of the 2D trapezoidal lattice becomes an analog of a 1D OBC chain, and supports an OBC type of HSTE, with a vanishing distribution on the other side of the corner, i.e., the top geometric edge of the trapezoidal lattice. This is because this edge acts as a part of the bulk and hence behaves as a vacuum for the skin-topological states. We note that such a geometric-dependent behavior arises from an effective PBC-OBC transition for the 1D boundary system, induced by the competition between boundary nonreciprocal pumping toward different chiral directions, which manifests as the two types of nontrivial higher-order topological phenomena along the boundary of the system. This is essentially different from the geometry-dependent bulk NHSE rooted in anisotropic properties of bulk spectral winding, manifesting as emergence or disappearance of NHSE for OBC along different directions [42].

To characterize this geometry-dependent behavior, we demonstrate the difference between ρ_{eff} and ρ_{edge} in Fig. 3(g), defined as

$$\Delta\rho = \sum_x |\rho_{\text{eff}} - \rho_{\text{edge}}|/L_{\text{eff}}$$

with L_{eff} the size of the 1D boundary system. It is seen that $\Delta\rho$ reaches its minimal value at around $M = 15$ for $t_a = 0.25$, the parameter chosen in other figures. With larger t_a, edge states of a breathing Kagome lattice become less localized along its 1D boundary, and their distributions also slightly diverge from that of the 1D boundary system, as shown by the increasing minimal value of $\Delta\rho$ in Fig. 3(g). In Supplemental Material [56], we further demonstrate examples of hexagon lattices, which also exhibit HSTE and boundary spectral winding similar to trapezoid lattices, and effective OBC and IBC for their 1D edges can be more clearly identified from a Green's function analysis.

V. DETECTION OF BOUNDARY SPECTRAL WINDING THROUGH A TOPOLOGICAL RESPONSE

In 1D non-Hermitian systems, it has been recently revealed that nontrivial spectral winding has a one-to-one correspondence to a quantized quantity in response to an external local driving field [34]. Despite that its generalization to higher-dimensional systems is still unclear, a similar topological response corresponding to the boundary spectral winding can be expected to emerge here, since edge states of our 2D model effectively give a 1D boundary system. Specifically, the topological response quantity is defined as

$$\nu_{mn}(\beta) = \partial \ln |G_{mn}(\beta)|/\partial\beta,$$

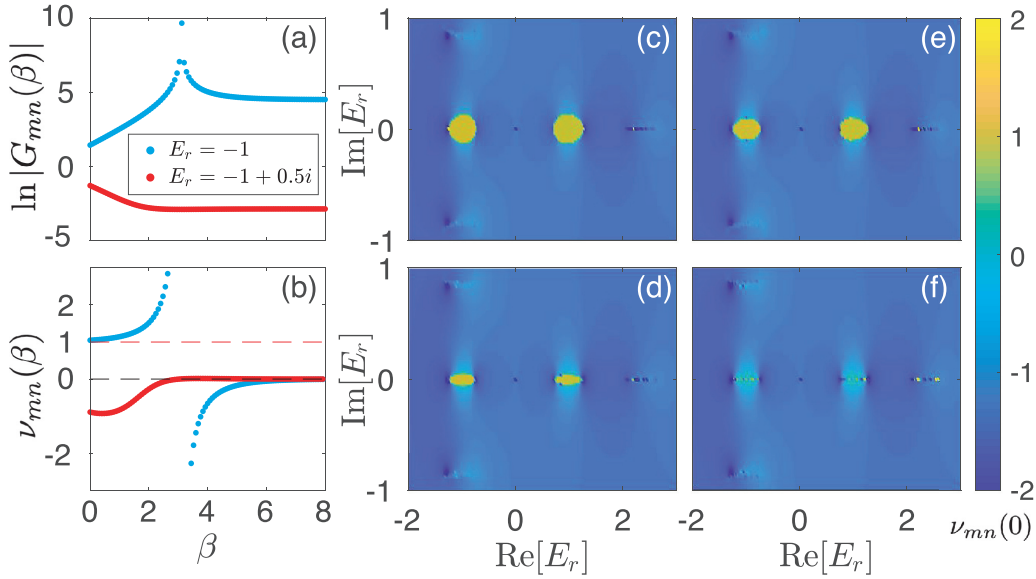

FIG. 4. (a) Element $G_{mn}(\beta)$ of the Green's function for the triangle lattice with the same parameters as in Fig. 1(a), for different reference energies E_r enclosed by the looplike boundary spectrum (blue dots) and within the gap (red dots), respectively. (b) Topological response $\nu_{mn}(\beta)$ for the same system and parameters as in (a). (c)–(f) Topological response $\nu_{mn}(\beta)$ at $\beta = 0$ for (c) the triangle lattice with $L = 30$ rows of unit cells and (d)–(f) the trapezoidal lattices for Figs. 3(d)–3(f) $M = 5, 10,$ and 20 rows removed from the triangle lattice, respectively. In all these results, m and n are chosen as the bottom-left and -right sites of the 15th unit cell in the bottom row of the lattices.

with β describing a perturbation to the amplitude of one intracell hopping along the system's 1D boundary $t_a \to t_a e^{-\beta}$, $G(\beta) = 1/[E_r - H(\beta)]$ the Green's function regarding a reference energy E_r, and (m, n) labeling the two sites connected by the perturbed hopping. By definition, $G(\beta)$ involves all eigenstates of $H(\beta)$ (which can be seen as an effective Hamiltonian from the quantum master equation [21]), and those with eigenenergies closer to E_r shall have larger contributions. We note that to obtain a topological response for the boundary spectral winding, the modified hopping can be chosen arbitrarily from the 1D boundary for the triangle lattice, but cannot be chosen from the top row of a trapezoidal lattice, which belongs to the bulk system [56]. In the following discussion, it is chosen to locate at the center of the bottom boundary. Physically, $|G_{mn}(\beta)|$ describes the amplitude of a response at site m to a local driving field at site n [21], thus $\nu_{mn}(\beta)$ describes the changing rate of this response strength with varying β [56]. We first consider the triangle lattice with the same parameters as in Fig. 2. As seen in Figs. 4(a) and 4(b), $G_{mn}(\beta)$ and $\nu_{mn}(\beta)$ behave rather differently for reference energies inside (blue) and outside (red) the loops of the boundary spectrum. For the former case, $|G_{mn}(\beta)|$ increases with β and eventually stops at a large constant value ($\approx e^5$), analogous to the direction signal amplification 1D non-Hermitian system [20,21]. In contrast, $|G_{mn}(\beta)|$ decreases to a small value ($\approx e^{-3}$) for a reference energy outside the loops of the boundary spectrum. More importantly, it is seen that $\nu_{mn}(\beta) \simeq 1$ [$\nu_{mn}(\beta) \leqslant 0$] for small β when E_r is (not) enclosed by the loops of the boundary spectrum, consistent with the quantized topological response in actual 1D systems [34–36]. Therefore we scan E_r for a parameter regime covering the system's full spectrum, and demonstrate the value of $\nu_{mn}(\beta)$ at $\beta = 0$ in Fig. 4(c). As seen in the results, the region with nontrivial boundary spectral winding is characterized by $\nu_{mn}(0) \simeq 1$, while other regions generally have a nonpositive $\nu_{mn}(0)$. Furthermore, in Figs. 4(e) and 4(f) we demonstrate the same response quantity $\nu_{mn}(\beta)$ for trapezoidal lattices with the same lattice size and parameters as in Figs. 3(d)–3(f). The nontrivial region is seen to shrink and disappear for trapezoidal lattices when removing more rows of unit cells, which perfectly matches the boundary spectra displayed in Figs. 3(d)–3(f).

VI. CONCLUSION

In summary, we highlight a boundary spectral winding in 2D non-Hermitian systems under the OBC, originating from the interplay between Hermitian (topological) boundary localization and non-Hermitian nonreciprocal pumping. The mechanism is similar to that of the HSTE, yet these two phenomena require rather different boundary geometric properties. Specifically, nontrivial boundary spectral winding naturally arises in a triangle lattice of a non-Hermitian breathing Kagome model, where a destructive interference of nonreciprocity along three directions ensures chiral nonreciprocal pumping along the 1D boundary of the lattice. On the other hand, a trapezoidal lattice of the same model supports different directions of nonreciprocal pumping for different parts of its boundary, leading to either a boundary spectral winding with a weak corner localization of edge states or an OBC type of HSTE, depending on the exact shape of the trapezoidal lattice. In both cases, we find that the boundary spectral winding can be detected from a topological response to a local driving field in the presence of a local boundary perturbation, established from an element of the Green's function matrix associating the response and the driven lattice sites. Our model is ready for experimental realization with *RLC* circuit lattices, as it is constructed with the same hopping components as several non-Hermitian lattices already

realized in this platform [60–62]. The topological response ν_{mn} can also be detected in such systems by measuring the two-point impedance between sites m and n, which takes a similar form of the Green's function [34]. As further verified in our Supplemental Material [56], the boundary spectral winding and its corresponding topological response are also robust against a relatively strong disorder. We also note that while this Letter has focused on a non-Hermitian breathing Kagome model with triangle and trapezoidal geometries, the boundary spectral winding shall also emerge in other models and geometries, as long as the boundary states experience certain non-Hermitian chiral pumping. Several examples are demonstrated in the Supplemental Material [56].

Note added. Recently, we became aware of Ref. [63], where boundary spectral winding topology emerges for eigenvalues of the Floquet operator of a Hermitian system.

ACKNOWLEDGMENTS

L.L. would like to thank C. H. Lee, J. Gong, and W. Zhu for helpful discussion. This work is supported by the National Natural Science Foundation of China (Grant No. 12104519) and the Guangdong Basic and Applied Basic Research Foundation (Grant No. 2020A1515110773).

[1] M. Z. Hasan and C. L. Kane, Colloquium: Topological insulators, Rev. Mod. Phys. **82**, 3045 (2010).
[2] X.-L. Qi and S.-C. Zhang, Topological insulators and superconductors, Rev. Mod. Phys. **83**, 1057 (2011).
[3] S. Yao and Z. Wang, Edge States and Topological Invariants of Non-Hermitian Systems, Phys. Rev. Lett. **121**, 086803 (2018).
[4] S. Yao, F. Song, and Z. Wang, Non-Hermitian Chern Bands, Phys. Rev. Lett. **121**, 136802 (2018).
[5] D. S. Borgnia, A. J. Kruchkov, and R.-J. Slager, Non-Hermitian Boundary Modes and Topology, Phys. Rev. Lett. **124**, 056802 (2020).
[6] K. Zhang, Z. Yang, and C. Fang, Correspondence between Winding Numbers and Skin Modes in Non-Hermitian Systems, Phys. Rev. Lett. **125**, 126402 (2020).
[7] N. Okuma, K. Kawabata, K. Shiozaki, and M. Sato, Topological Origin of Non-Hermitian Skin Effects, Phys. Rev. Lett. **124**, 086801 (2020).
[8] T. E. Lee, Anomalous Edge State in a Non-Hermitian Lattice, Phys. Rev. Lett. **116**, 133903 (2016).
[9] Y. Xiong, Why does bulk boundary correspondence fail in some non-Hermitian topological models, J. Phys. Commun. **2**, 035043 (2018).
[10] F. K. Kunst, E. Edvardsson, J. C. Budich, and E. J. Bergholtz, Biorthogonal Bulk-Boundary Correspondence in Non-Hermitian Systems, Phys. Rev. Lett. **121**, 026808 (2018).
[11] K. Yokomizo and S. Murakami, Non-Bloch Band Theory of Non-Hermitian Systems, Phys. Rev. Lett. **123**, 066404 (2019).
[12] Z. Yang, K. Zhang, C. Fang, and J. Hu, Non-Hermitian Bulk-Boundary Correspondence and Auxiliary Generalized Brillouin Zone Theory, Phys. Rev. Lett. **125**, 226402 (2020).
[13] C. H. Lee and R. Thomale, Anatomy of skin modes and topology in non-Hermitian systems, Phys. Rev. B **99**, 201103(R) (2019).
[14] L. Herviou, J. H. Bardarson, and N. Regnault, Defining a bulk-edge correspondence for non-Hermitian Hamiltonians via singular-value decomposition, Phys. Rev. A **99**, 052118 (2019).
[15] S. Longhi, Topological Phase Transition in Non-Hermitian Quasicrystals, Phys. Rev. Lett. **122**, 237601 (2019).
[16] H. Jiang, L.-J. Lang, C. Yang, S.-L. Zhu, and S. Chen, Interplay of non-Hermitian skin effects and Anderson localization in nonreciprocal quasiperiodic lattices, Phys. Rev. B **100**, 054301 (2019).
[17] F. Song, S. Yao, and Z. Wang, Non-Hermitian Skin Effect and Chiral Damping in Open Quantum Systems, Phys. Rev. Lett. **123**, 170401 (2019).
[18] F. Song, S. Yao, and Z. Wang, Non-Hermitian Topological Invariants in Real Space, Phys. Rev. Lett. **123**, 246801 (2019).
[19] S. Weidemann, M. Kremer, T. Helbig, T. Hofmann, A. Stegmaier, M. Greiter, R. Thomale, and A. Szameit, Topological funneling of light, Science **368**, 311 (2020).
[20] C. C. Wanjura, M. Brunelli, and A. Nunnenkamp, Topological framework for directional amplification in driven-dissipative cavity arrays, Nat. Commun. **11**, 3149 (2020).
[21] W.-T. Xue, M.-R. Li, Y.-M. Hu, F. Song, and Z. Wang, Simple formulas of directional amplification from non-Bloch band theory, Phys. Rev. B **103**, L241408 (2021).
[22] C. C. Wanjura, M. Brunelli, and A. Nunnenkamp, Correspondence between Non-Hermitian Topology and Directional Amplification in the Presence of Disorder, Phys. Rev. Lett. **127**, 213601 (2021).
[23] J. C. Budich and E. J. Bergholtz, Non-Hermitian Topological Sensors, Phys. Rev. Lett. **125**, 180403 (2020).
[24] K. Wang, A. Dutt, K. Y. Yang, C. C. Wojcik, J. Vučković, and S. Fan, Generating arbitrary topological windings of a non-Hermitian band, Science **371**, 1240 (2021).
[25] S. Longhi, Self-Healing of Non-Hermitian Topological Skin Modes, Phys. Rev. Lett. **128**, 157601 (2022).
[26] S. Mu, C. H. Lee, L. Li, and J. Gong, Emergent Fermi surface in a many-body non-Hermitian fermionic chain, Phys. Rev. B **102**, 081115(R) (2020).
[27] C. H. Lee, L. Li, R. Thomale, and J. Gong, Unraveling non-Hermitian pumping: Emergent spectral singularities and anomalous responses, Phys. Rev. B **102**, 085151 (2020).
[28] C. H. Lee, Exceptional Bound States and Negative Entanglement Entropy, Phys. Rev. Lett. **128**, 010402 (2022).
[29] C.-X. Guo, C.-H. Liu, X.-M. Zhao, Y. Liu, and S. Chen, Exact Solution of Non-Hermitian Systems with Generalized Boundary Conditions: Size-Dependent Boundary Effect and Fragility of the Skin Effect, Phys. Rev. Lett. **127**, 116801 (2021).
[30] Y. Yi and Z. Yang, Non-Hermitian Skin Modes Induced by On-Site Dissipations and Chiral Tunneling Effect, Phys. Rev. Lett. **125**, 186802 (2020).
[31] L. Li, C. H. Lee, and J. Gong, Impurity induced scale-free localization, Commun. Phys. **4**, 1 (2021).

[32] L. Li, C. H. Lee, and J. Gong, Geometric characterization of non-Hermitian topological systems through the singularity ring in pseudospin vector space, Phys. Rev. B **100**, 075403 (2019).
[33] L. Li, C. H. Lee, S. Mu, and J. Gong, Critical non-Hermitian skin effect, Nat. Commun. **11**, 5491 (2020).
[34] L. Li, S. Mu, C. H. Lee, and J. Gong, Quantized classical response from spectral winding topology, Nat. Commun. **12**, 5294 (2021).
[35] Y. Liu, Y. Zeng, L. Li, and S. Chen, Exact solution of the single impurity problem in nonreciprocal lattices: Impurity-induced size-dependent non-Hermitian skin effect, Phys. Rev. B **104**, 085401 (2021).
[36] H.-Q. Liang, S. Mu, J. Gong, and L. Li, Anomalous hybridization of spectral winding topology in quantized steady-state responses, Phys. Rev. B **105**, L241402 (2022).
[37] L. Li and C. H. Lee, Non-Hermitian pseudo-gaps, Sci. Bull. **67**, 685 (2022).
[38] X.-Q. Sun, P. Zhu, and T. L. Hughes, Geometric Response and Disclination-Induced Skin Effects in Non-Hermitian Systems, Phys. Rev. Lett. **127**, 066401 (2021).
[39] B. A. Bhargava, I. C. Fulga, J. van den Brink, and A. G. Moghaddam, Non-Hermitian skin effect of dislocations and its topological origin, Phys. Rev. B **104**, L241402 (2021).
[40] F. Schindler and A. Prem, Dislocation non-Hermitian skin effect, Phys. Rev. B **104**, L161106 (2021).
[41] A. Panigrahi, R. Moessner, and B. Roy, Non-Hermitian dislocation modes: Stability and melting across exceptional points, Phys. Rev. B **106**, L041302 (2022).
[42] K. Zhang, Z. Yang, and C. Fang, Universal non-Hermitian skin effect in two and higher dimensions, Nat. Commun. **13**, 2496 (2022).
[43] H. Jiang and C. H. Lee, Dimensional transmutation from non-Hermiticity, arXiv:2207.08843v2.
[44] K. Kawabata, M. Sato, and K. Shiozaki, Higher-order non-Hermitian skin effect, Phys. Rev. B **102**, 205118 (2020).
[45] S. A. A. Ghorashi, T. Li, M. Sato, and T. L. Hughesc, Non-Hermitian higher-order Dirac semimetals, Phys. Rev. B **104**, L161116 (2021).
[46] C. H. Lee, L. Li, and J. Gong, Hybrid Higher-Order Skin-Topological Modes in Nonreciprocal Systems, Phys. Rev. Lett. **123**, 016805 (2019).
[47] L. Li, C. H. Lee, and J. Gong, Topological Switch for Non-Hermitian Skin Effect in Cold-Atom Systems with Loss, Phys. Rev. Lett. **124**, 250402 (2020).
[48] Y. Li, C. Liang, C. Wang, C. Lu, and Y.-C. Liu, Gain-Loss-Induced Hybrid Skin-Topological Effect, Phys. Rev. Lett. **128**, 223903 (2022).
[49] W. Zhu and J. Gong, Hybrid skin-topological modes without asymmetric couplings, Phys. Rev. B **106**, 035425 (2022).
[50] Y. Fu, J. Hu, and S. Wan, Non-Hermitian second-order skin and topological modes, Phys. Rev. B **103**, 045420 (2021).
[51] R. Okugawa, R. Takahashi, and K. Yokomizo, Second-order topological non-Hermitian skin effects, Phys. Rev. B **102**, 241202(R) (2020).
[52] E. Edvardsson, F. K. Kunst, and E. J. Bergholtz, Non-Hermitian extensions of higher-order topological phases and their biorthogonal bulk-boundary correspondence, Phys. Rev. B **99**, 081302(R) (2019).
[53] W. P. Su, J. R. Schrieffer, and A. J. Heeger, Solitons in Polyacetylene, Phys. Rev. Lett. **42**, 1698 (1979).
[54] S. Lieu, Topological phases in the non-Hermitian Su-Schrieffer-Heeger model, Phys. Rev. B **97**, 045106 (2018).
[55] C. Yin, H. Jiang, L. Li, R. Lü, and S. Chen, Geometrical meaning of winding number and its characterization of topological phases in one-dimensional chiral non-Hermitian systems, Phys. Rev. A **97**, 052115 (2018).
[56] See Supplemental Material at http://link.aps.org/supplemental/10.1103/PhysRevB.107.L161404 for more details about boundary states of our non-Hermitian breathing Kagome model, the model under hexagonal geometries, topological boundary response for driving fields at different locations, results of a non-Hermitian Benalcazar-Bernevig-Hughes model, and the effect of disorder in our system, which includes Refs. [20,21,57–59].
[57] W. A. Benalcazar, B. A. Bernevig, and T. L. Hughes, Quantized electric multipole insulators, Science **357**, 61 (2017).
[58] W. A. Benalcazar, B. A. Bernevig, and T. L. Hughes, Electric multipole moments, topological multipole moment pumping, and chiral hinge states in crystalline insulators, Phys. Rev. B **96**, 245115 (2017).
[59] P. W. Anderson, Absence of diffusion in certain random lattices, Phys. Rev. **109**, 1492 (1958).
[60] T. Helbig, T. Hofmann, S. Imhof, M. Abdelghany, T. Kiessling, L. W. Molenkamp, C. H. Lee, A. Szameit, M. Greiter, and R. Thomale, Generalized bulk-boundary correspondence in non-Hermitian topolectrical circuits, Nat. Phys. **16**, 747 (2020).
[61] T. Hofmann, T. Helbig, F. Schindler, N. Salgo, M. Brzezińska, M. Greiter, T. Kiessling, D. Wolf, A. Vollhardt, A. Kabaši *et al.*, Reciprocal skin effect and its realization in a topolectrical circuit, Phys. Rev. Res. **2**, 023265 (2020).
[62] D. Zou, T. Chen, W. He, J. Bao, C. H. Lee, H. Sun, and X. Zhang, Observation of hybrid higher-order skin-topological effect in non-Hermitian topolectrical circuits, Nat. Commun. **12**, 7201 (2021).
[63] H. Liu and I. C. Fulga, Mixed higher-order topology: boundary non-Hermitian skin effect induced by a Floquet bulk, arXiv:2210.03097v1.